

ANALYSIS OF A CONICAL SLEEVE WITH PIVOT JOINT LOADING OF AXIAL FORCE

ANDRZEJ ANDRZEJKU, ZBIGNIEW SKUP, ROBERT ZALEWSKI

Warsaw University of Technology, Institute of Machine Design Fundamentals, Warszawa, Poland

e-mail: mang@ipbm.simr.pw.pl; zskup@ipbm.simr.pw.pl; robertzalewski@wp.pl

The paper presents theoretical and experimental studies of energy dissipation in a model of a conical sleeve-pivot joint. Energy dissipation between cooperating surfaces of a friction pair including structural friction, elastic and frictional effects between its elements and Lame's problem are taken into account. A comparative analysis was conducted to compare the theoretical results obtained from numerical simulations and direct experimental data acquired from the MTS testing machine. The analysis of the influence of geometrical and material parameters, external loading on the dissipation of energy is presented too. This paper shows an outline of theoretical considerations, the method for conducting tests as well as selected comparative results.

Keywords: conical joint, hysteresis loop, experimental testing

1. Introduction

Analytical considerations concern the natural energy dissipation problem observed on a temporary fastening in a conical sleeve-pivot joint subject to an axial load. In the literature, the authors have not found papers concerning the problem of natural damping of vibrations in a conical sleeve-pivot joints (including structural damping). The range of the present paper includes theoretical and experimental investigations of the previously mentioned assemblies subjected to the axial loading. Such a type of friction joints can be commonly found in various mechanical systems used in daily engineering applications, e.g. machine tools, automobile or aircraft industry. In this paper, authors investigate a fastening with Coulomb's law, elasticity of the joint elements, Saint-Venant's principle and Lame's problem taken into account. Beside theoretical tests, also a mathematical model, based on the a real experimental research, is proposed and verified. The sleeve-pivot connection shown in Fig. 2a was subjected to an axial load αP ($0 \leq \alpha \leq \alpha_1$). In this paper, an assumption has been made that $\alpha_1 = 1$. The main aim of the theoretical investigation is a detailed analysis of the previously mentioned conical joint taking into consideration structural friction, which appears in a temporary and permanent fastening everywhere, where a step out pressure acts onto cooperating surfaces. Energy dissipation phenomena caused by structural friction is observed in various types of wedge connections in both temporary and permanent joints. This problem is widely discussed in the literature for more than fifty years. The pioneer work that considered static problems for structural friction with additional simplified assumptions was done by Kalinin *et al.* (1960). Thereafter, similar problems were investigated in both the domestic and foreign literature. It is worth mentioning that static and dynamic problems observed in the structural friction field were particularly considered in monographs e.g. by Giergiel (1990), Osiński (1986, 1998), Skup (2010) and papers by Gałkowski (1999), Grudziński and Kostek (2005), Kaczmarek (2003), Sadowski and Stupkiewicz (2010) or Kosior (2005). The examples of references by other foreign authors include works of Ando *et al.* (1995), Feeny *et al.* (1998), Lin and Cai (1990), Person (1998), Popp (1998), Sextro (2002). The static analysis of different types of cooperating joints is generally limited to investigations of displacements in an

external loading function or determination of the static hysteresis loop (Fig. 1). The structural friction phenomenon is rather a complex problem mainly due to: sophisticated mathematical description of the structural friction phenomenon, loads and stresses distribution, nonlinearities of strains and functions describing the structural hysteresis loop, roughness of the contacting surfaces, etc.

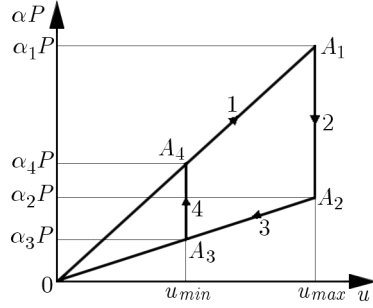


Fig. 1. Theoretical hysteresis loop of the sleeve-pivot joint

2. Determination of the axial displacement in function of an external load for loading stages of the sleeve-pivot joint

A simplified model of a sleeve-pivot joint loaded by an axial force αP is shown in Fig. 2a. Displacements in the loaded sleeve-pivot joint have been examined in four different loading stages. In each stage, an amount of dissipated energy was investigated. The section of the tested object, having height Δx has been depicted in Fig. 2. Theoretical considerations have been taken separately for the sleeve and pivot. In the next step, the authors established a mathematical formulation for the whole assembly.

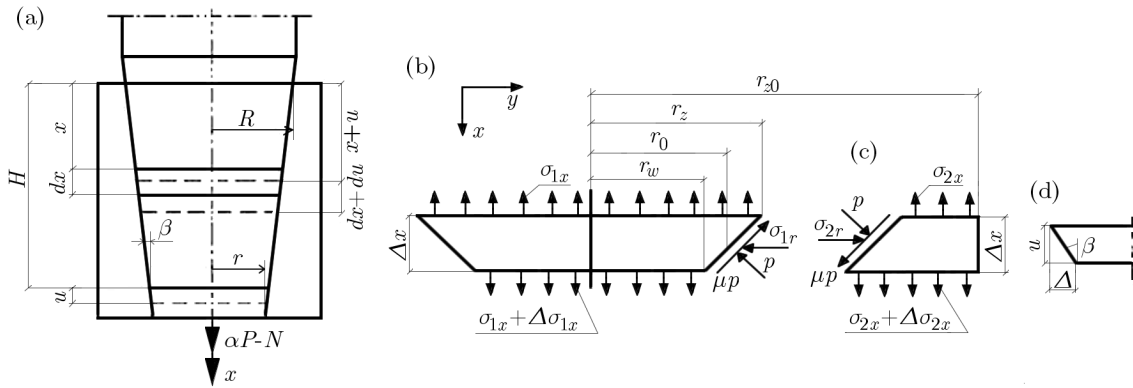


Fig. 2. Physical model: (a) sleeve-pivot joint, (b) section of the pivot, (c) section of the sleeve, (d) displacement scheme

Stage 1 – Loading of the sleeve-pivot joint section (Fig. 2a) ($0 \leq \alpha P \leq \alpha_1 P$)

The external radius r_0 of the joint section (Fig. 2b) can be defined as

$$r_0 = R - x \tan \beta \quad (2.1)$$

The force equilibrium equation in the section of the investigated sleeve-pivot joint is

$$\Delta \sigma_{1x} F_1 = \Delta \sigma_{2x} F_2 \rightarrow \Delta \sigma_{2x} = \frac{r_0^2}{r_{z0}^2 - r_0^2} \Delta \sigma_{1x} \quad (2.2)$$

where: F_1, F_2 are the fields of the cross-sectional area of the pivot and sleeve section, $\Delta\sigma_{1x}, \Delta\sigma_{2x}$ – increase of normal stresses in the considered sleeve and pivot.

Considerations for the pivot section (Fig. 2b)

The equation of the equilibrium from the projection of forces in the x -axial direction can be described as

$$-\sigma_{1x}\pi r_0^2 - \mu p \cos \beta 2\pi r_0 \frac{\Delta x}{\cos \beta} - p \sin \beta 2\pi r_0 \frac{\Delta x}{\cos \beta} + (\sigma_{1x} + \Delta\sigma_{1x})\pi r_0^2 = 0 \quad (2.3)$$

where μ is the friction coefficient.

From transformed equation (2.3) and formula (2.2), the pressure per unit value p for the contact surface joint is given by

$$p = \frac{\Delta\sigma_{1x}}{\Delta x} \frac{r_0}{2(\tan \beta + \mu)} \quad (2.4)$$

The equation of the equilibrium of forces operating in the pivot section in the radial direction (y -axis, Fig. 2b) is

$$(-\sigma_{1r} + \mu p \sin \beta - p \cos \beta) 2\pi r_0 \frac{\Delta x}{\cos \beta} = 0 \quad (2.5)$$

Substituting formula (2.4) into equation (2.5), the radial stresses are

$$\sigma_{1r} = \frac{-r_0 \cos \beta (1 - \mu \tan \beta)}{2(\mu + \tan \beta)} \frac{\Delta\sigma_{1x}}{\Delta x} \quad (2.6)$$

Taking into account the symmetry of the system in the axial direction of x, y , and z (Fig. 2bc), and in accordance with Hooke's law (Dylag *et al.*, 1996), the relative radial strain ε_{1r} was determined

$$\sigma_{1z} = \sigma_{1y} = \sigma_{1r} \quad \varepsilon_{1z} = \varepsilon_{1y} = \varepsilon_{1r} \quad \varepsilon_{1z} = \frac{1}{E_1} [\sigma_{1z} - \nu_1 (\sigma_{1x} + \sigma_{1y})] \quad (2.7)$$

Taking into consideration dependences (2.7), equation (2.7)₃ takes the form

$$\varepsilon_{1r} = \frac{\sigma_{1r}(1 - \nu_1)}{E_1} - \frac{\nu_1 \sigma_{1x}}{E_1} \quad (2.8)$$

where ν_1, E_1 are Poisson's ratio and Young's modulus of the pivot section.

As a result of the radial deformation of the pivot section, its radius changes. Its absolute radial displacement can be described after substituting formula (2.6) into equation (2.8) by the formula

$$\Delta r_{01} = \varepsilon_{1r} r_0 = \frac{-r_0^2 \cos \beta (1 - \mu \tan \beta)(1 - \nu_1)}{2E_1(\mu + \tan \beta)} \frac{\Delta\sigma_{1x}}{\Delta x} - \frac{\nu_1 r_0 \sigma_{1x}}{E_1} \quad (2.9)$$

Considerations for the sleeve section (Fig. 2c)

The equation of the equilibrium from the projection of forces in the x -axial direction takes the form

$$-\sigma_{2x}\pi(r_{z0}^2 - r_0^2) + \mu p \cos \beta 2\pi r_0 \frac{\Delta x}{\cos \beta} + p \sin \beta 2\pi r_0 \frac{\Delta x}{\cos \beta} + (\sigma_{2x} + \Delta\sigma_{2x})\pi(r_{z0}^2 - r_0^2) = 0 \quad (2.10)$$

By transforming, reducing and substituting dependence (2.2), a formula describing pressure per unit at the contact surface joint can be defined as in Eq. (2.4).

The equation of the equilibrium from the projection of forces in the y -radial direction (Fig. 2b) takes the form

$$(\sigma_{2r} - \mu p \sin \beta + p \cos \beta) 2\pi r_0 \frac{\Delta x}{\cos \beta} = 0 \quad (2.11)$$

hence, it appears

$$\sigma_{2r} = -p \cos \beta (1 - \mu \tan \beta) = p_a \quad (2.12)$$

The distribution of stresses σ_{2r} and displacements u_p (Fig. 3) in the radial direction can be determined by using Lame's problem formulas (Dylag *et al.*, 1997), thus

$$\sigma_{2r} = \frac{E_2}{1 - \nu_2^2} \left(C_1 (1 + \nu_2) - \frac{C_2}{r^2} (1 - \nu_2) \right) \quad u_p = C_1 r + \frac{C_2}{r} \quad (2.13)$$

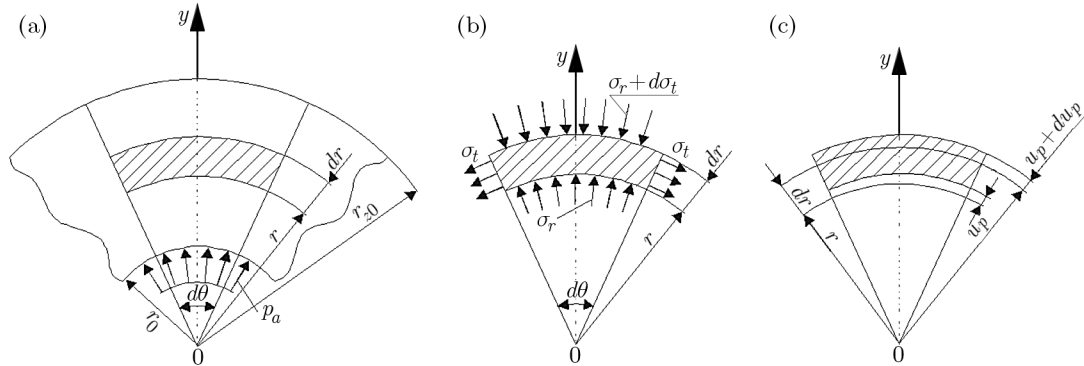


Fig. 3. Axially symmetrical stresses and displacements in the sleeve section

The integration constants C_1 and C_2 occurring in (2.13)₁ were determined with the following boundary conditions

$$\sigma_{2r} = \begin{cases} -p_a = p \cos \beta (1 - \mu \tan \beta) & \text{for } r = r_0 \\ 0 & \text{for } r = r_{z0} \end{cases} \quad (2.14)$$

Therefore

$$C_1 = \frac{(1 - \nu_2)r_0^2 \cos \beta p (1 - \mu \tan \beta)}{E_2(r_0^2 - r_{z0}^2)} \quad C_2 = \frac{(1 + \nu_2)r_0^2 r_{z0}^2 \cos \beta p (1 - \mu \tan \beta)}{E_2(r_0^2 - r_{z0}^2)} \quad (2.15)$$

Substituting dependences (2.15) in (2.13)₁, a formula describing the radial stresses in the sleeve section was obtained in the following form

$$\sigma_{2r} = \frac{r_0^2 \cos \beta p (1 - \mu \tan \beta)}{r_0^2 - r_{z0}^2} \left(1 - \frac{r_{z0}^2}{r^2} \right) \quad (2.16)$$

Next, the radial displacement u_p (Fig. 2c) was determined from equation (2.13)₂, additionally taking into consideration integration constants (2.15)

$$u_p = \frac{r_0^2 \cos \beta p (1 - \mu \tan \beta)}{E_2(r_0^2 - r_{z0}^2)} \left((1 - \nu_2)r + (1 + \nu_2) \frac{r_{z0}^2}{r} \right) \quad (2.17)$$

Finally, for $r = r_0$ from (2.4), formula (2.17) after transformations can also be written in another form

$$u_p|_{r=r_0} = \frac{-r_0^4 \cos \beta (1 - \mu \tan \beta)}{2E_2(r_0^2 - r_{z0}^2)(\tan \beta + \mu)} \left((1 - \nu_2) + \frac{r_{z0}^2}{r_0^2} (1 + \nu_2) \right) \frac{\Delta \sigma_{1x}}{\Delta x} \quad (2.18)$$

The displacement Δ between the cooperating surface elements of the joint (Fig. 2), by making use of formulas (2.9) and (2.18), is given by

$$\Delta = u_p|_{r=r_0} - \Delta r_{01} = \frac{\Delta \sigma_{1x}}{\Delta x} z_1 + \sigma_{1x} \frac{\nu_1 r_0}{E_1} \quad (2.19)$$

where

$$z_1 = \frac{r_0^2 \cos \beta}{2} \frac{1 - \mu \tan \beta}{\tan \beta + \mu} \left[\frac{-r_0^2}{E_2(r_0^2 - r_{z0}^2)} \left(1 - \nu_2 + \frac{r_{z0}^2}{r_0^2} (1 + \nu_2) \right) + \frac{1 - \nu_1}{E_1} \right] \quad (2.20)$$

A mutual axial displacement of the pivot and sleeve joint sections (Fig. 2) for the first stage of the loading can be described as follows

$$u = \frac{\Delta}{\tan \beta} = \frac{\Delta \sigma_{1x}}{\Delta x} \frac{z_1}{\tan \beta} + \sigma_{1x} \frac{\nu_1 r_0}{E_1 \tan \beta} \quad (2.21)$$

thus formula (2.21) through making use of formula (2.20) takes the form

$$u_1 = \eta_3(R - x \tan \beta)^2 \sigma'_{1x} + \eta_4(R - x \tan \beta) \sigma_{1x} \quad (2.22)$$

where

$$\begin{aligned} \eta_1 &= \frac{\chi}{E_2} \left(1 - \nu_2 + \frac{r_{z0}^2}{r^2} (1 + \nu_2) \right) + \frac{1 - \nu_1}{E_1} & \eta_2 &= \frac{\cos \beta (1 - \mu \tan \beta)}{2(\tan \beta + \mu) \tan \beta} \\ \eta_3 &= \eta_1 \eta_2 & \eta_4 &= \frac{\nu_1}{E_1 \tan \beta} & \chi &= \frac{1}{\left(\frac{r_{z0}}{r} \right)^2} - 1 \end{aligned} \quad (2.23)$$

therefore, the axial strain displacement derivative (formula (2.22)) with respect to the distance x gives:

$$\varepsilon_{1x} = \frac{du_1}{dx} = \eta_3(R - x \tan \beta)^2 \sigma''_{1x} + (R - x \tan \beta)(\eta_4 - 2\eta_3 \tan \beta) \sigma'_{1x} - \eta_4 \tan \beta \sigma_{1x} \quad (2.24)$$

The relationship between the stresses and axial strains according to Hooke's law is

$$\varepsilon_{1x} = \frac{1}{E_1} [\sigma_{1x} - \nu_1 (\sigma_{1z} + \sigma_{1y})] \quad (2.25)$$

Taking into account the symmetry of the system, formula (2.7)_{1,2} takes the form

$$\varepsilon_{1x} = \frac{\sigma_{1x}}{E_1} - 2\sigma_{1r} \frac{\nu_1}{E_1} \quad (2.26)$$

After substituting equations (2.1) and (2.6) in (2.26) and transformisg, we get

$$\varepsilon_{1x} = \frac{\sigma_{1x}}{E_1} + \eta_5(R - x \tan \beta) \sigma'_{1x} \quad \eta_5 = \frac{\nu_1 \cos \beta (1 - \mu \tan \beta)}{E_1 (\tan \beta + \mu)} \quad (2.27)$$

Comparing formula (2.24) to (2.27), a homogeneous quadratic differential equation with variable coefficients has been obtained

$$\begin{aligned} \eta_3(R - x \tan \beta)^2 \sigma''_{1x} + \eta_6(R - x \tan \beta) \sigma'_{1x} - \eta_7 \sigma_{1x} &= 0 \\ \eta_6 &= \eta_4 - 2\eta_3 \tan \beta - \eta_5 & \eta_7 &= \eta_4 \tan \beta + \frac{1}{E_1} \end{aligned} \quad (2.28)$$

Substituting $\sigma_{1x} = (R - x \tan \beta)^\lambda$ into (2.28), the characteristic equation is given by

$$\lambda^2 - B_4\lambda - C_{12} = 0 \quad B_4 = 1 + \frac{\eta_6}{\eta_3 \tan \beta} \quad C_{12} = \frac{\eta_7}{\eta_3} \tan^2 \beta \quad (2.29)$$

the characteristic equation discriminant is

$$\Delta_{41} = B_4^2 + 4C_{12} > 0 \quad \lambda_{9,10} = \frac{B_4 \mp \sqrt{\Delta_{41}}}{2} \quad (2.30)$$

therefore, the general solution to the differential equation may be written in the form

$$\sigma_{1x} = C_{13}(R - x \tan \beta)^{\lambda_9} + C_{14}(R - x \tan \beta)^{\lambda_{10}} \quad (2.31)$$

The integration constants C_{13} and C_{14} were designated for the next boundary conditions, thus

$$\sigma_{1x} = \begin{cases} 0 & \text{for } x = 0 \\ \frac{\alpha P}{\pi r^2} & \text{for } x = H \end{cases} \quad (2.32)$$

therefore

$$C_{13} = -C_{14}R^{\lambda_{10}-\lambda_9} \quad C_{14} = \frac{\alpha P}{\pi r^2(r^{\lambda_{10}} - R^{\lambda_{10}-\lambda_9}r^{\lambda_9})} \quad r = R - H \tan \beta \quad (2.33)$$

Finally

$$\sigma_{1x} = C_{14}[(R - x \tan \beta)^{\lambda_{10}} - (R - x \tan \beta)^{\lambda_9}R^{\lambda_{10}-\lambda_9}] \quad (2.34)$$

The stress derivative is given by

$$\sigma'_{1x} = C_{14} \tan \beta [\lambda_9 R^{\lambda_{10}-\lambda_9} (R - x \tan \beta)^{\lambda_9-1} - \lambda_{10} (R - x \tan \beta)^{\lambda_{10}-1}] \quad (2.35)$$

Considering $x = H$, we get

$$\sigma'_{1x}(x = H) = C_{14} \tan \beta (\lambda_9 R^{\lambda_{10}-\lambda_9} r^{\lambda_9-1} - \lambda_{10} r^{\lambda_{10}-1}) \quad (2.36)$$

Substituting obtained solutions (2.33), (2.32), (2.34) and (2.36)) in equation (2.22) depending on the operating external force αP , the formula of displacement of the extreme cross-section ($x = H$) takes the form

$$u_1(x = H) = \frac{\alpha P}{\pi r} \left(\eta_4 + \frac{\eta_3 \tan \beta (\lambda_9 R^{\lambda_{10}-\lambda_9} r^{\lambda_9} - \lambda_{10} r^{\lambda_{10}})}{r^{\lambda_{10}} - R^{\lambda_{10}-\lambda_9} r^{\lambda_9}} \right) \quad (2.37)$$

Formula (2.37) describes the loading process of the investigated sleeve-pivot joint depicted in Fig. 1, interval 1.

Stage 2 – Unloading of the sleeve-pivot joint section without sliding

$$(\alpha_2 P \leq \alpha P \leq \alpha_1 P)$$

Unloading of the investigated system consists of decreasing the force value from $\alpha_1 P$ down to $\alpha_2 P$. This stage is represented in Fig. 1 as a straight line $A_1 A_2$ (interval 2). This process does not produce any changes in the value of displacement.

Stage 3 – Unloading of the sleeve-pivot joint section with sliding

$$(\alpha_3 P \leq \alpha P \leq \alpha_2 P)$$

If we consider the friction forces per unit value equal to $-\mu p$ acting on the considered slice (the stress is equal to σ_x), the sliding phenomenon of cooperating surfaces will occur. The loading state of the investigated joint at this stage is depicted in Fig. 4. Similarly to the first stage, formulas are obtained for the unloading process.

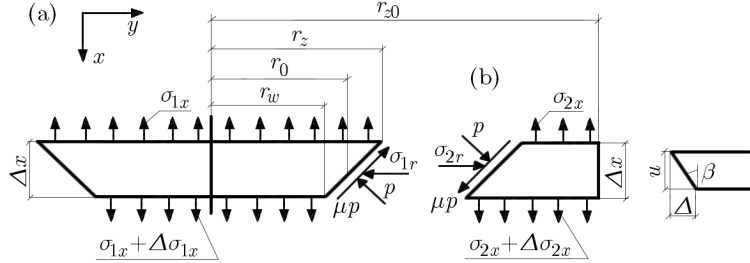


Fig. 4. The unloading of the object (a) pivot sector, (b) sleeve sector

Considerations for the pivot section (Fig. 4a)

The equation of equilibrium of forces operating in the joint along the x -axis (Fig. 4a) takes the following form

$$-\sigma_{1x}\pi r_0^2 - p \sin \beta 2\pi r_0 \frac{\Delta x}{\cos \beta} + \mu p \cos \beta 2\pi r_0 \frac{\Delta x}{\cos \beta} + (\sigma_{1x} + \Delta\sigma_{1x})\pi r_0^2 = 0 \quad (2.38)$$

The equation of the equilibrium of forces in the radial direction on the y -axis (Fig. 4a) is given by

$$(-\sigma_{1r} - \mu p \sin \beta - p \cos \beta)2\pi r_0 \frac{\Delta x}{\cos \beta} = 0 \quad (2.39)$$

Considerations for a sleeve section (Fig. 4b)

Considering the equilibrium of force in the horizontal direction (Fig. 4b), we get

$$-\sigma_{2x}\pi(r_{z0}^2 - r_0^2) - \mu p \cos \beta 2\pi r_0 \frac{\Delta x}{\cos \beta} + p \sin \beta 2\pi r_0 \frac{\Delta x}{\cos \beta} + (\sigma_{2x} + \Delta\sigma_{2x})\pi(r_{z0}^2 - r_0^2) = 0 \quad (2.40)$$

The equation of the equilibrium of forces in the radial direction on the y -axis (Fig. 4b) takes the following form

$$(\sigma_{2r} + \mu p \sin \beta + p \cos \beta)2\pi r_0 \frac{\Delta x}{\cos \beta} = 0 \quad (2.41)$$

Similarly to the first stage, the axial displacement in the third stage ($u_3(x = H)$) may be written in the form

$$u_3(x = H) = \frac{\alpha P}{\pi r} \left(\eta_4 + \frac{\eta_9 \tan \beta (\lambda_{11} R^{\lambda_{12}-\lambda_{11}} r^{\lambda_{11}} - \lambda_{12} r^{\lambda_{12}})}{r^{\lambda_{12}} - R^{\lambda_{12}-\lambda_{11}} r^{\lambda_{11}}} \right) \quad (2.42)$$

where

$$\begin{aligned} \eta_9 &= \eta_1 \eta_8 & \eta_8 &= \frac{\cos \beta (1 + \mu \tan \beta)}{2 \tan \beta (\tan \beta - \mu)} & \lambda_{11,12} &= \frac{B_5 \mp \sqrt{\Delta_{43}}}{2} \\ \Delta_{43} &= B_5^2 + 4C_{15} > 0 & B_5 &= 1 + \frac{\eta_{10}}{\eta_9 \tan \beta} & \eta_{10} &= \eta_4 - 2\eta_9 \tan \beta - c_1 \\ c_1 &= \frac{\nu_1 \cos \beta (1 + \mu \tan \beta)}{E_1 (\tan \beta - \mu)} & C_{15} &= \frac{\eta_7}{\eta_9 \tan^2 \beta} \end{aligned}$$

Formula (2.42) describes the unloading process of the sleeve-pivot joint, depicted in Fig. 1 (interval 3).

Stage 4 – Reloading process of the investigated joint ($\alpha_3 P \leq \alpha P \leq \alpha_4 P$)

At the initial moment of the reloading process $\alpha_3 P$ to $\alpha_4 P$, we do not observe the movement of cooperating elements in the investigated joint. The constant displacement is continued until the friction forces μp change the sign (Fig. 1, interval 4).

3. Determining of the energy dissipation for a single loading cycle of the investigated system

During a single loading cycle, the amount of dissipated in the system energy can be expressed by $\int \alpha P(u) du$ and corresponds to the field of the hysteresis loop in the triangular form OA_1A_2 or the quadrangle form $A_1A_2A_3A_4$ ($\alpha_3 > 0$) (Fig. 1), depending on the loading method of the investigated system.

The amount of energy dissipation for the single loading cycle (Fig. 1) can be given in the following form

$$\psi = \frac{P}{2}u_{max}(\alpha_1 - \alpha_2) - \frac{P}{2}u_{min}(\alpha_4 - \alpha_3) \quad (3.1)$$

Assuming $\alpha = \alpha_1$ and independent from α parameters $\eta_1-\eta_9, r, R, \lambda_9-\lambda_{12}, \beta, H$, formula (2.37) takes the form

$$u_1(x = H) = u_{1\ max} = \alpha_1 P(m_{17} + m_{18}) \quad (3.2)$$

and for $\alpha = \alpha_2$, formula (2.42) is given by

$$u_3(x = H) = u_{3\ max} = \alpha_2 P(m_{19} + m_{18}) \quad (3.3)$$

where

$$\begin{aligned} m_{17} &= \frac{\eta_3 \tan \beta (\lambda_9 R^{\lambda_{10}-\lambda_9} r^{\lambda_9} - \lambda_{10} r^{\lambda_{10}})}{\pi r (r^{\lambda_{10}} - R^{\lambda_{10}-\lambda_9} r^{\lambda_9})} & m_{18} &= \frac{\eta_4}{\pi r} \\ m_{19} &= \frac{\eta_9 \tan \beta (\lambda_{11} R^{\lambda_{12}-\lambda_{11}} r^{\lambda_{11}} - \lambda_{12} r^{\lambda_{12}})}{\pi r (r^{\lambda_{12}} - R^{\lambda_{12}-\lambda_{11}} r^{\lambda_{11}})} \end{aligned} \quad (3.4)$$

Comparing formulas (3.2) and (3.3), we get

$$\alpha_2 = \alpha_1 \frac{m_{17} + m_{18}}{m_{19} + m_{18}} \quad (3.5)$$

Assuming $\alpha = \alpha_4$, formula (2.37) takes the form

$$u_1(x = H) = u_{1\ min} = \alpha_4 P(m_{17} + m_{18}) \quad (3.6)$$

For $\alpha = \alpha_3$, formula (2.42) is given by

$$u_3(x = H) = u_{3\ min} = \alpha_3 P(m_{19} + m_{18}) \quad (3.7)$$

Similarly – for stage 4, when the friction forces change their direction, α_4 value was determined by comparison of formulas (3.6) and (3.7), therefore

$$\alpha_4 = \alpha_3 \frac{m_{19} + m_{18}}{m_{17} + m_{18}} \quad (3.8)$$

Finally substituting expressions (3.2), (3.5), (3.7) and (3.8) in formula (3.1). we get

$$\psi = \frac{P^2}{2} (m_{19} - m_{17}) \left(\alpha_1^2 \frac{m_{17} + m_{18}}{m_{19} + m_{18}} - \alpha_3^2 \frac{m_{19} + m_{18}}{m_{17} + m_{18}} \right) \quad (3.9)$$

4. Results of numerical simulations

Simulation tests were carried out in the Mathematica 6.1 environment. The numerical calculations were conducted assuming the following values of parameters taken directly from the experimental setup: $\nu_1 = \nu_2 = 0.29$, $E_1 = E_2 = 2.1 \cdot 10^{11} \text{ N/m}^2$, $\mu = 0.15$, $\beta = 12^\circ, 14^\circ, 16^\circ, 18^\circ$, $R = 38 \cdot 10^{-3} \text{ m}$, $r = 28.03 \cdot 10^{-3} \text{ m}$, $H = 40 \cdot 10^{-3} \text{ m}$.

As a result of numerical calculations, hysteresis loops were obtained for both frictional and elastic models (Figs. 5 and 6) of the cooperating elements. Additionally, Lame's problem has been taken into account.

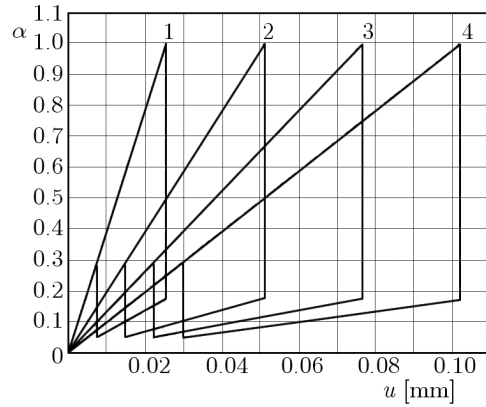


Fig. 5. Structural hysteresis loops for the frictional sleeve-pivot model for various loading values P :
1 – 25 kN, 2 – 50 kN, 3 – 75 kN, 4 – 100 kN and $\beta = 12^\circ$, $v = 0.29$, $\mu = 0.15$

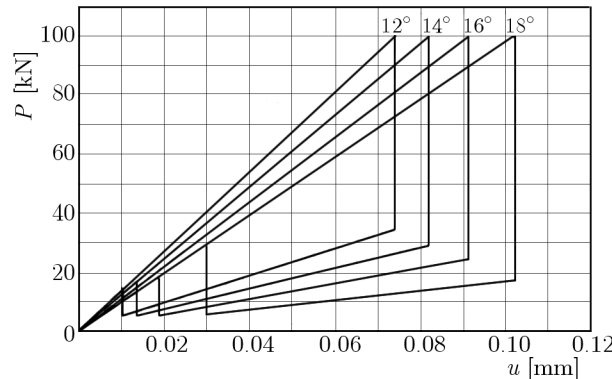


Fig. 6. Hysteresis loops for different values of coning angles of the friction joint; $v = 0.29$, $\mu = 0.15$

the data depicted in Figs. 5 and 6 enable comparison of the amount of energy dissipated in the investigated joint for various load values (Fig. 5) and cone angle values (Fig. 6). Analyzing the results, we can observe that higher values of the loading forces result in increasing of the investigated displacement and the amount of energy dissipated in the system (Fig. 5).

The conducted numerical tests revealed that the increasing of the cone angle β results in linear decreasing of the structural hysteresis loop area (Fig. 6). Detailed analysis of the data depicted in Fig. 7 enabled determination of the optimal value of the friction coefficient ($\mu = 0.13$) assuming the highest amount of the dissipated energy criteria.

The data depicted in Fig. 8 reveals characteristics of the hysteresis loop area ψ in function of the loading force P . Numerically acquired characteristics $\psi(P)$ have strongly nonlinear character for all considered cone angle values. Analyzing the data presented in Fig. 8, one can observe that the obtained characteristics $\psi(P)$ are nonlinear for different values of coning angles.

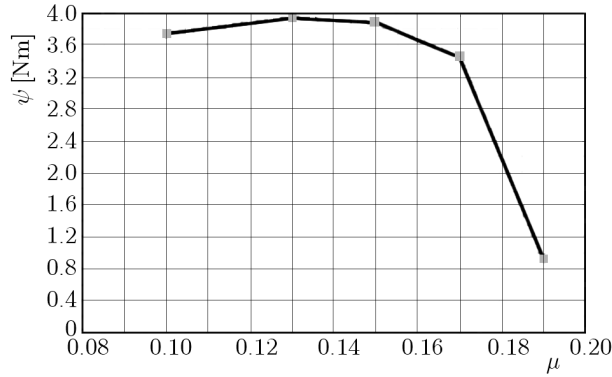


Fig. 7. Energy losses in function of the friction coefficient for the unloading process of the tested model; $P = 100 \text{ kN}$, $\beta = 12^\circ$, $v = 0.29$

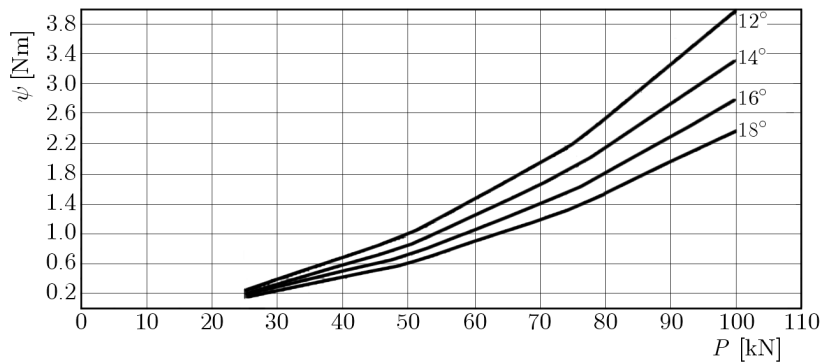


Fig. 8. Energy losses in function of the loading for various values of the cone angle β of the investigated system; $v = 0.29$, $\mu = 0.15$

As a conclusion, it is worth mentioning that in the design process of material systems and constructions including friction cone joints, it is possible to use the natural way of vibration damping by using structural friction occurring in the friction cone joint. The obtained results confirmed that by an appropriate selection of geometrical parameters of the tested joint (for example Fig. 6 or Fig. 8) and material properties (for example Fig. 7), the amount of natural energy dissipated in the investigated system can reach its highest possible value.

The obtained results have confirmed that conducting such kind of experimental and numerical tests can be very useful. The presented in the paper analytical considerations allow one – at the initial stage of design – to examine vibration damping strategies without involving the real model of the expensive cone joint element. Such an approach seems to be especially reasonable from the economical point of view.

5. The experimental model

The main goal of experimental testing is to choose the most suitable mathematical model that would constitute the best approximation of the real model response, i.e. minimizing the differences between the areas of experimental and numerical hysteresis loops. In order to perform experimental tests, a real model of the friction pair of the sleeve-pivot joint was designed and manufactured (Fig. 9). The experimentally investigated model was made of steel S2. In the testing specimen, a cone angle $\beta = 14^\circ$ was applied. The overall construction model is shown in Fig. 9. It was designed in such a way that its position in the machine gripping jaws during the loading process would not change (Fig. 9 – elements 3 and 4). To measure displacements of the

system, extensometers 2 and 3 (Fig. 10) were used with a measurement base of 10 mm and a measurement nominal range ± 1.2 mm (sub-range of the nominal range ± 0.24 mm), which were included in the standard equipment of the universal strength testing machine MTS 809 (Fig. 10 – elements 2, 3).

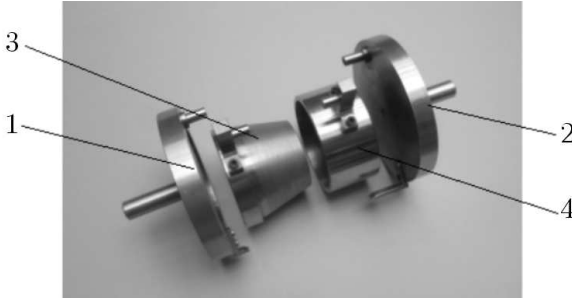


Fig. 9. Design of the experimental model of a sleeve-pivot friction joint (decomposed system): 1 – lower pressure plate grip, 2 – upper grip, 3 – pivot, 4 – sleeve

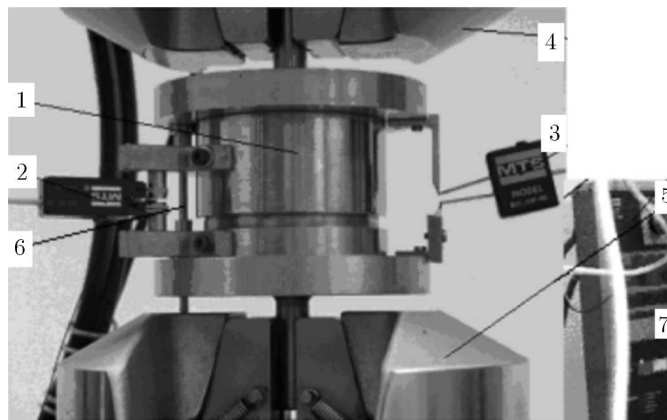


Fig. 10. Fastening of the tested model and an overview of its components: 1 – sleeve-pivot, 2 – extensometer type Ext_26, 3 – extensometer type Ext COD; 4, 5 – upper and lower gripping jaws of the MTS testing machine, 6 – steady pin, 7 – programmer

The method of fastening extensometers 2 and 3 (Fig. 10) to tested elements 3 and 4 (Fig. 9) is illustrated in Fig. 10. In elements 3 and 4 (Fig. 9), a steady pin was mounted in order to ensure a coaxial measurement base for extensometers 2 and 3 (Fig. 10). In order to provide the best conditions for the cooperating joined elements (maximum contact surface, surface pressure, smoothness of the motion), the conical surfaces were subject to a surface finishing process that consisted of very precise grinding.

6. The results of experimental testing

The tests were conducted using the MTS testing machine at the Institute of Machine Design Fundamentals of Warsaw University of Technology. In the measurements, the Test Ware SX special software has been used. The fastening scheme of the investigated system is illustrated in Fig. 10. The single measurement methodology consisted of initial loading the system up to a maximal force value P_{max} limited by safety loading threshold of the tested material (elastic range of deformations). Next, the system was unloaded down to the pre-assumed value P_{min} and reloaded again. The loading process was fully controlled by the computer to avoid arising the torque while the experiment was conducted. Each experimental test was preceded by the

calibration processes of both the extensometer and the control-measurement system. All experimental data, acquired from the laboratory tests was transformed into suitable characteristics plotted in the Mathematica 6.1 software. (Figs. 11 and 12). The same numerical environment was applied to approximate the obtained graphs and to calculate the area of experimental hysteresis loops with a numerical integration method. Typical experimental results are depicted in Figs. 11 and 12. The system was loaded up to $P_{max} = 25, 50, 75, 100 kN, and then unloaded to $P_{min} = 5 kN.$$

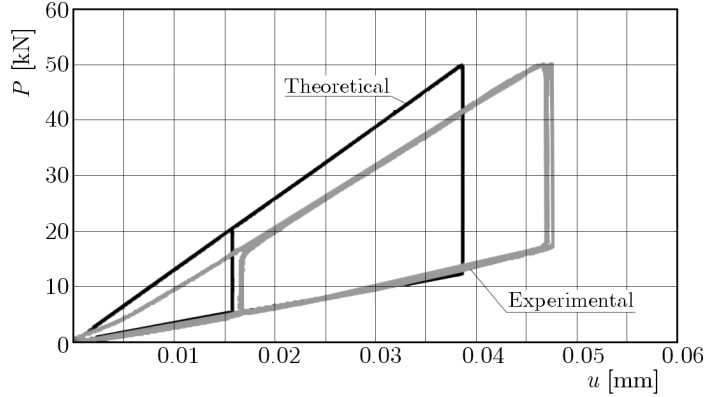


Fig. 11. Verification of the experimental and numerical data for $P_{max} = 50 kN,
number of loading cycles: 4$

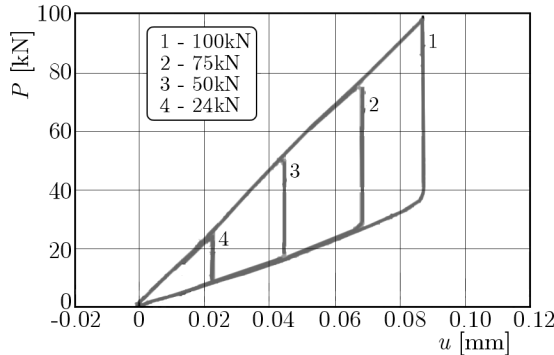


Fig. 12. Experimental hysteresis loops for the model loaded by various forces P_{max} ,
number of loading cycles: 4

In Fig. 12, a set of experimentally determined hysteresis loops has been depicted. The previously mentioned characteristics have been obtained for various loading forces P_{max} from 25 kN to 100 kN, and a constant unloading condition $P_{min} = \text{const} = 5 kN.$

The loading program realized on the tensile strength machine consisted of linear increasing of the compression force value up to P_{max} value, maintaining the maximal load for 10 s, and unloading process down to the threshold value P_{min} . Four independent loading cycles have been realized.

It has to be mentioned, that the described loading process of the cone joint is very complex. It is quite difficult to separate the structural friction phenomenon from the experimental data mainly due to the existence of internal friction, which was neglected in the theoretical considerations.

Table 1 shows the comparison of energy losses obtained as a result of numerical simulations and real experimental tests and the percentage difference between them.

Table 1. The percentage difference between average values of experimental and numerical hysteresis loop areas

No.	Load [KN]	Theoretical model ψ [Nm]	Experimental model ψ [Nm]	Difference [%]
1	25	207.192	166.64	19.57
2	50	827.716	767.95	7.22
3	75	1862.360	1739.08	6.62
4	100	3310.860	3113.04	5.97

7. Conclusions

The paper presents a mathematical model of the sleeve-pivot cone joint and results of numerical simulations and experimental tests conducted on a real model. A comparative analysis allows one to formulate a conclusion that the numerical response of the model reflects the real behaviour of the investigated cone joint. The characteristics depicted in Fig. 11 are comparable – both quantitatively and qualitatively. The divergence between the theoretical and experimental results is mainly caused by the simplifying assumptions taken for the mathematical model, i.e. constant friction coefficient, negligence of internal friction, precision of manufacturing of the real model, problems related to the fixing of the model in the testing machine (positioning of the model in gripping jaws of the testing machine) and problems encountered during measurements.

References

1. ANDO Y., ISHIKAWA Y., KITAHARA T., 1995, Friction characteristics and adhesion under low normal load, *Journal of Tribology*, **117**, 569-574
2. DYLĄG Z., JAKUBOWICZ A., ORŁOŚ Z., 1996, 1997, *Strength of Materials* (in Polish), vol. I and II, Publishers Technical of Science, Warsaw
3. FEENY B., GURAN A., HINRICHES N., POPP K., 1998, A historical review on dry friction and stick-slip phenomena, *Applied Mechanics Review*, **51**, 321-341
4. GAŁKOWSKI Z., 1999, Influence of structural friction of the vibrations sleeve-shaft (in Polish), *Science of Books Rzeszów University of Technology*, **174**, 283-288
5. GIERGIEL J., 1990, *Damping of Mechanical Vibrations* (in Polish), Polish Publishers of Science, Warsaw
6. GRUDZIŃSKI K., KOSTEK R., 2005, Influence of normal micro-vibrations in contact on sliding motion of solid body, *Journal of Theoretical and Applied Mechanics*, **43**, 37-49
7. KACZMAREK W., 2003, Analysis of a bolted joint with elastic and frictional effects occurring between its elements, *Machine Dynamics Problems*, **27**, 1, 21-40
8. KALININ N., LEBIEDIEW JU., PANOWKO J.G., LEBIEDIEW V.J., STRACHOW G.I., 1961, *Konstrukcyonnoe dempfirovaniye v nepodvizhnykh soedineniyakh*, Akademija Nauk Łatwijskoj CCR, Riga
9. KOSIOR A., 2005, *Influence of Parameters of Joints with Structural Friction on Elastic and Damping Properties of Mechanical Systems*, Publishing House of the Warsaw University of Technology, Mechanics, Exercise, book 209
10. LIN Y.K., CAI G.Q., 1990, *Random Vibration of Hysteresis Systems, Nonlinear Dynamics in Engineering Systems*, Springer Verlag, Berlin, Heidelberg, 189-196
11. PERSON B.N.J., 1998, *Sliding Friction*, Springer, Berlin
12. POPP K., 1998, A historical review on dry friction and stick-slip phenomena, *Applied Mechanics Review*, **51**, 321-341

13. OSIŃSKI Z., 1986, *Damping of Mechanical Vibrations* (in Polish), Polish Publishing House, Warsaw
14. OSIŃSKI Z., 1988, *Damping of Vibrations*, A.A. BALKEMA/Rotterdam/Brookfield
15. SADOWSKI P., STUPKIEWICZ S., 2010, Combined effect of friction and macroscopic deformation on asperity flattening, *Tribology International*, **43**, 9, 1735-1741
16. SEXTRO W., 2002, *Dynamical Contact Problems with Friction*, Springer, Berlin
17. SKUP Z., 2010, *Nonlinear Phenomena in the Damping Vibration* (in Polish), Publishing House of the Warsaw University of Technology, pp. 376

Manuscript received May 14, 2013; accepted for print October 14, 2013